MODELLING THE THERMAL DECOMPOSITION OF CARBON FIBRE MATERIALS DURING RE-ENTRY

B. Fritsche

HTG, 37191 Katlenburg-Lindau, Germany, Email: B.Fritsche@htg-hst.de

ABSTRACT

The SCARAB software is a tool for calculating the motion and aerothermal destruction of spacecraft entering the Earth's atmosphere. To increase the accuracy of the re-entry simulation for spacecraft containing CFRP as wall material, the modelling of the properties of CFRP was improved. Different to the simple conventional "metallic" model with monolithic properties a sophisticated model with different zones with different properties and taking into account additional effects was developed. First a mathematical model was formulated, which was then converted to a numerical model. The numerical 1D model was tested in a testbed software, then implemented into the SCARAB software and applied to wind tunnel conditions and the re-entry of the ROSAT satellite.

Key words: CFRP; Ablation; SCARAB; Re-entry.

1. INTRODUCTION

The SCARAB software ("Spacecraft Atmospheric Re-entry and Aerothermal Break-up") [1] has been developed and applied now for more than 15 years to simulate the re-entry motion and the associated mechanical and thermal destruction of spacecraft during their re-entry into the Earth's atmosphere. Up to now the modelling of the thermal destruction process was based on the assumption that the materials of the spacecraft parts behave like metals, i.e. that they are heated by the incoming aerothermal heat flux according to their specific heat capacity up to their melting temperature, then melt according to their specific heat of melting up to demise. As it is known and proven by wind tunnel tests not all solid spacecraft materials can be modelled like metals. This is especially true and important for CFRP (Carbon fibre reinforced plastic) which can be an abundant material in some spacecraft structures. The main difference to metals is that CFRP does not melt (except at very high temperatures which are not reached during a normal re-entry from Earth orbit) but first decomposes by an endothermic process (pyrolysis) and then burns in an exothermic process (oxidation). Both processes remove material from the wall. There are even additional processes which can remove material from the surface (erosion, sublimation). The sum of all effects can be considered as "ablation".

This paper describes how the ablation mechanism was included in the SCARAB software to extend its possibilities to model a larger class of materials. As a first step a one-dimensional (1D) model of the ablation process was developed. On the 1D level these algorithms were adopted in SCARAB. Due to the 3D nature of the model and motion simulation in SCARAB there was additional effort required to incorporate the 1D model in an adequate manner into the whole simulation. The 1D model was compared to windtunnel tests with cylindrical probes. The 3D implementation in SCARAB was applied to the re-entry simulation of the ROSAT satellite.

2. 1D ABLATION MODEL

2.1. Mathematical Formulation

CFRP consists of a mixture of two solids: a carbon fibre with embedded epoxy resin. When a CFRP wall is heated from one side e.g. during re-entry its temperature increases and the epoxy filler (or the phenolic resin) close to the surface starts to decompose into gaseous pyrolysis products by endothermic chemical reactions. The decomposition layer travels with increasing temperature into the "virgin" material. On the backside of this decomposition layer remains a porous carbon char through which the pyrolysis gases escape into the external flow. The outflow of pyrolysis gases into the hot boundary layer reduces the aerodynamic heat transfer rate. On the surface the carbon char is also oxidized by impinging oxygen, which produces additional heating.

A thermal analysis of such a problem consists of a simultaneous calculation of the changes of local temperature and mass as response to the action of thermal loads and to the local thermal state. For a thermal model of the ablation process each effect to be considered has its own response function. The mathematical concept presented in this paper is based mainly on [2], see also [3].

Proc. '6th European Conference on Space Debris'
Darmstadt, Germany, 22–25 April 2013 (ESA SP-723, August 2013)

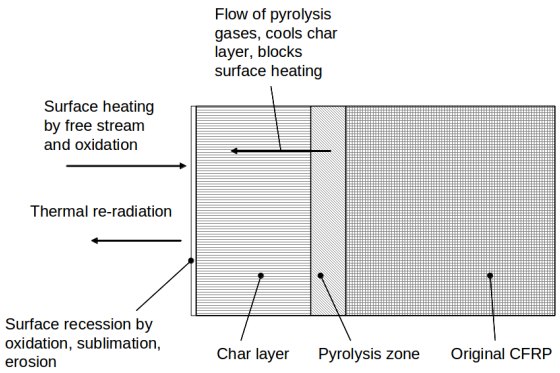

Figure 1. Processes modelled with the 1D ablation model.

2.1.1. Heating, Radiation, Heat Conduction and Melting

The local heating at a given position in a material by incoming heat $\dot{q}_h$ is given by the equation

$$\frac{\partial \dot{q}_h}{\partial x} = \rho c_p \dot{T} \tag{1}$$

ρ, c_p and T are the local values of density, specific heat ratio and temperature.

If the local temperature exceeds the local melting temperature, the material melts at a rate (h_{melt} is the melting enthalpy)

$$\dot{s} = \dot{q}_h / (\rho h_{melt}) \tag{2}$$

Surfaces at temperatur T can re-radiate heat to the outside.

$$\dot{q}_r = \sigma \epsilon T^4 \tag{3}$$

$\sigma = 5.67 \cdot 10^{-8}$ W/(m^{2}K^4) is the Stefan-Boltzmann constant and ϵ is the emissivity of the material.

Between internal surfaces heat can be exchanged by heat conduction (λ is the local conductivity)

$$\dot{q}_c = -\lambda \frac{\partial T}{\partial x} \tag{4}$$

2.1.2. Pyrolysis

Pyrolysis denotes the process of decomposition of the epoxy resin embedded in the carbon fibre to gaseous reaction products. The reaction diminishes the partial mass density ρ_p of the resin:

$$\dot{\rho}_p = -F \rho_p \tag{5}$$

where F is a reaction rate depending on temperature:

$$F = \sum_i A_i \exp(-E_i / (\Re T)) \tag{6}$$

with rate constants A_i, activation energies E_i and universal gas constant $\Re = 8314$ J/(K mole). The pyrolysis is an endothermic process, which adds a negative heat flux to the local heat balance:

$$\dot{q}_p = h_p \dot{\rho}_p \tag{7}$$

where h_p denotes the heat of pyrolysis.

Due to mass conservation the gaseous reaction products are generated with the same rate as the epoxy is removed. Due to their much higher volume they will quickly move out of the pyrolysis zone and flow through the charred front region finally out of the heated solid. This has several additional effects.

Change of local properties Due to the local mass loss after outflow the local thermal properties are changed by the pyrolysis process.

Heat exchange with char layer On their way through the charred region the pyrolysis gases can exchange heat in this region:

$$\dot{q}_g = \dot{m}_g c_{p,g} \frac{\partial T}{\partial x} \tag{8}$$

$\dot{m}_g$ is the mass flux and $c_{p,g}$ is the specific heat capacity of the pyrolysis gases.

Blowing On outflow through the frontal surface the pyrolysis gases change the flow field in front of the surface and hence the external aerodynamic heat input $\dot{q}_\infty$. This can be accounted for by a blowing factor, which is a measure for the reduction of the effective aerothermal heat flux.

$$\dot{q}_{\infty,\phi} = \phi \dot{q}_\infty \tag{9}$$

ϕ can vary between 0 and 1. Under certain assumptions the blowing factor can be calculated by

$$\phi = \frac{aB}{e^{aB} - 1} \tag{10}$$

with

$$B = \frac{\dot{m}_{ox} + \dot{m}_g}{\dot{q}_\infty / (h_0 - h_w)} \tag{11}$$

where $\dot{m}_{ox}$ and $\dot{m}_g$ are the mass fluxes generated by oxidation and pyrolysis, and h_0 and h_w are the total aerodynamic enthalpy and the wall enthalpy. The constant a depends on the gas, the flow conditions and the Mach number. For CFRP a reasonable value is $a = 1.3$.

Erosion On outflow through the front surface the pyrolysis gases can blow apart small carbon fibres. This is difficult to model in detail. In [2] a very simple correlation for the mass loss by erosion $\dot{m}_{blow}$ was found experimentally:

$$\dot{m}_{blow} = \dot{m}_g / x_{blow} \tag{12}$$

with the constant x_{blow} determined from experiments.

2.1.3. Oxidation and Sublimation

After a local layer is pyrolysed a carbon char layer remains. If the incoming free stream contains oxygen, the front surface of the charred region can react with the oxygen, generating gaseous carbon oxide molecules which leave the surface, thus recessing the front layer by oxidation at a rate $\dot{m}_{ox}$ which depends on the oxigen flux impinging onto the front surface and the oxigen reaction rate. This process is exothermic and results in an additional external heating rate of (h_{ox} is the heat of oxidation)

$$\dot{q}_{ox} = \dot{m}_{ox} h_{ox} \tag{13}$$

Another process specific to charred CFRP compared to metals is the process of sublimation. This process would compare to evaporation on metal surfaces. Metals will melt before they can loose significant mass by evaporation. This is different for carbon, which has a very high melting temperature. An order of magnitude analysis however shows, that sublimation for CFRP becomes significant only for temperatures above 3000 K, which are not achieved during orbital spacecraft decays and can therefore be neglected in the current context.

2.2. Numerical Formulation

Having established the mathematical formulation for all effects to be considered a numerical formulation has to be set up. There are two fundamental principles in the transformation of a mathematical to a numerical approach:

1. Discretization in space. The spatial derivatives in the differential equations have to be approximated by spatial differences.

2. Discretization in time. Since it is not possible to compute the change of temperature and heat fluxes simultaneously, usually the temperature distribution given at some time instant is used to compute the heat fluxes. Then all heat fluxes are evaluated for each local numerical cell and the thermal response (temperature change etc.) in all cells is computed for the next time step. With the new thermal states the heat fluxes are computed and the procedure is repeated.

Both discretizations cannot be performed arbitrarily. They are coupled by the Fourier criterion:

$$Fo = a\Delta t/(\Delta x)^2 < 0.5 \tag{14}$$

with $a = \lambda/(c_p \rho)$, the thermal diffusivity, depending on local heat conductivity λ, heat capacity c_p and density ρ. In principle it is not predetermined how to discretize space and time. In practice the space discretization is selected in advance and the time discretization is adapted to the space discretization.

For the numerical algorithm the one-dimensional wall or slab is divided into a number of N layers of constant thickness d, numbered in the following by 1 to N, with 1 denoting the front surface. Since layers can be removed by recessing processes, the actual outside lying surface layer can have an index $i > 1$. This index will be denoted by i_s.

In the following the sequence of calculation steps is listed for each layer number i.

2.2.1. Heat Fluxes

Heat conduction Heat conduction takes place between two neighbor layers, if at least one of them is internal (neither on the surface, index i_s, nor on the backside, index N).

$$\dot{q}_{c,i} = 2 \cdot \frac{T_{i-1} - T_i}{d_i/\lambda_i + d_{i-1}/\lambda_{i-1}} + 2 \cdot \frac{T_{i+1} - T_i}{d_i/\lambda_i + d_{i+1}/\lambda_{i+1}} \tag{15}$$

External heating The external heating is the sum of all heat sources going into the surface layer. It is the sum of the re-radiation cooling, the aerodynamic heating and the oxidation heating, where the latter two are modified by the blowing factor.

$$\dot{q}_{x,i} = -\dot{q}_{rad} + (\dot{q}_{aero} + \dot{q}_{ox})\phi \tag{16}$$

Actually, $\dot{q}_{x,i}$ will only be non-zero for $i = i_s$.

Pyrolysis The pyrolysis contributes to the heat balance by the heat exchange with the pyrolysis gases generated in the pyrolysis zone flowing out through the char layer, and by the heat of pyrolysis needed to decompose the epoxy resin and to generate the pyrolysis gases.

The cooling by the gases passing through a layer is computed assuming that all pyrolysis gas generated during the previous time step flows through the layer and exchanges heat by adapting its temperature to the layer temperature.

$$\dot{q}_{g,i} = -\sum_{j=i+1}^{N} \dot{m}_{p,j} c_{pg} (T_i - T_{i+1}) \tag{17}$$

The cooling by decomposition of the epoxy is just proportional to the density change, which depends on the reaction rate.

$$\dot{q}_{p,i} = -F(T_i)\rho_{p,i} h_p \tag{18}$$

2.2.2. Thermal response

The thermal response comprises the change of state variables in the layer by the total heat input. It is computed as the sum of the heat fluxes above times the integration time step.

$$\dot{q}_i = \dot{q}_{c,i} + \dot{q}_{x,i} + \dot{q}_{g,i} + \dot{q}_{p,i} \tag{19}$$

$$\Delta q_i = \dot{q}_i \Delta t \tag{20}$$

Heating First a theoretical temperature change is computed, where in the heat capacity of the layer also the generated pyrolysis gas is considered.

$$\Delta T_i = \Delta q_i / ((c_{p,i}\rho_i + c_{pg}\rho_{pg,i})\, d_i) \tag{21}$$

If the computed temperature is below the melting temperature, it is accepted as new value for the layer.

Melting If the computed temperature is above the melting temperature, the growth of the meltlayer is computed.

$$\Delta s = \frac{T_i + \Delta T_i - T_{melt}}{\Delta T_i} \frac{\Delta q_i}{h_{melt}\rho_i} \tag{22}$$

Although melting does not play a role for CFRP ablation, it was included in the mathematical and numerical formulation and later in the implementation to make the layer concept also applicable to metals, especially for the case of low thermal conductivity. For metals there will be no pyrolysis considered, of course.

Pyrolysis From the pyrolysis reaction rate the new epoxy density is computed.

$$\Delta\rho_{p,i} = \dot{\rho}_{p,i} \Delta t \tag{23}$$

$$\dot{m}_{g,i} = -\dot{\rho}_{p,i} d_i \tag{24}$$

The sum of the generated pyrolysis gas flow is computed.

$$\dot{m}_g = \sum_i \dot{m}_{g,i} \tag{25}$$

Oxidation and Erosion From the external oxidation rate and the pyrolysis gas flow the surface recession is computed.

$$\dot{s} = (\dot{m}_{ox} + \dot{m}_g / x_{blow}) / \rho_C \tag{26}$$

2.3. Software Implementation

The numerical equations listed in the previous section can be implemented in a software to compute the 1D ablation of a substrate under the action of external heat loads. This was done by Kuch [2] to test the model by comparison with wind tunnel measurements, also fitting some physical parameters of the model. The implementation was realized there as MATLAB functions. For an implementation in SCARAB the MATLAB implementation could not be used, since the analysis modules of SCARAB are coded in FORTRAN, so the ablation model had to be re-coded anyway. This was done in two steps. First the 1D algorithm was coded in subroutines and a test main routine was written to test them in stand-alone mode. Then the subroutines were adapted to work in the frame of the SCARAB subroutine calling environment. Again a test main routine was written to test the subroutines in this environment. This is the wind tunnel mode of SCARAB. Finally the subroutines were linked to the complete SCARAB code, enabling SCARAB to compute spacecraft re-entries with ablation.

For testing of the 1D routines the different heat flux effects were switched on and off and the resulting temperature profiles were checked. In the following results of such sample calculations are shown. The material was assumed to be CFRP with 60% epoxy resin for the calculations including pyrolysis, and "charred" CFRP for all calculations without pyrolysis.

A constant external heat flux of 100 kW/m^2 was assumed. This is about one order of magnitude less than in the wind tunnel tests and at peak heating during re-entry. The wall thickness was 20 mm, divided into 10 layers. For the checking of the oxidation algorithm a constant thickness loss rate of 0.04 mm/s for oxidation (corresponding to complete oxidation of 1 layer in 50 seconds) and 0.02 mm/s (1 layer/100 s) for pyrolysis+oxidation was assumed. The initial temperature was 300 K for all cases and all layers.

Fig. 2 shows the simple case where only heat conduction is considered. In the front layers the temperature rises quite fast while the back layers need some time to respond to the incoming heat. After about 200 s the temperature rises in all layers at the same rate.

Fig. 3 shows the temperature history in the different layers when radiation from the front face is included. These profiles are significantly different from Fig. 2. At later times the temperatures are considerably damped. The outer layer does not reach 1200 K after 500 s, compared to 3000 K without radiation.

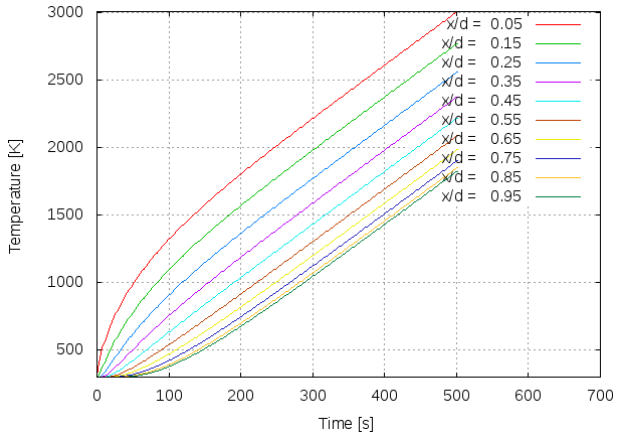

Figure 2. Heat conduction.

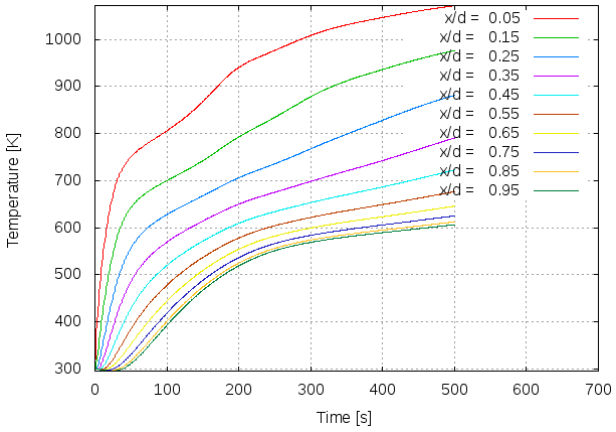

Figure 4. Heat conduction and radiation and pyrolysis.

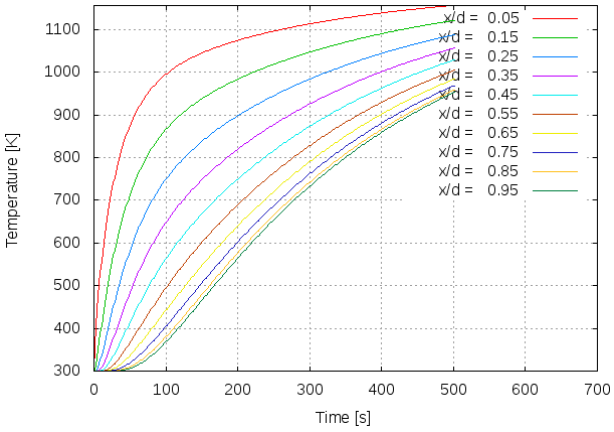

Figure 3. Heat conduction and radiation.

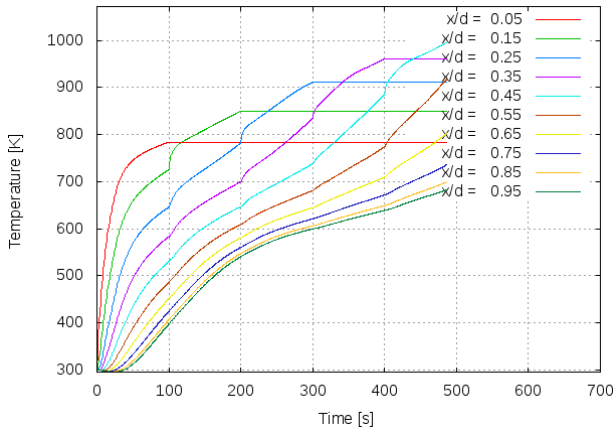

Figure 5. Heat conduction and radiation and pyrolysis and oxidation.

Fig. 4 shows the temperature profiles for conduction, radiation and pyrolysis. Compared to the case without pyrolysis the temperature profiles show peculiar variations. The pyrolysis is endothermic, therefore the temperatures are lower than without pyrolysis. The non-monotonic variation in the profiles can be accounted for by the pyrolysis energy which varies as function of temperature.

Fig. 5 shows the temperature profiles for conduction, radiation and pyrolysis and oxidation. The demise of the outer layers by the oxidation enhances the heat flux to the lower layers and increases their temperatures compared to the case without oxidation.

3. APPLICATIONS

3.1. Wind Tunnel Tests

In 2001 several material probes were tested in the arc-jet wind tunnel LBK in Cologne in simulated re-entry flow conditions [4]. The probes were spherical disks, with a diameter of 50 mm and a thickness of 20 mm. The materials used were Invar, Zerodur (high-temperature resistant glass), CFRP, Copper, and Aluminium. The temperature was measured on the surface with a pyrometer, within the probe with two thermocouples at 5 mm and 15 mm below the surface, and with one thermocouple at the probe's back.

While it is straightforward to compare such measurements with a pure 1D code, it is not that simple to compare them with the full SCARAB implementation, even for a 1D geometry. The reason is that SCARAB is designed to get its free-stream conditions from the actual conditions during a re-entry flight, which are computed from the flight dynamic and aerodynamic state of the spacecraft. For wind tunnel comparisons a special "wind tunnel mode" was established, using a dedicated interface and a subset of the simulation routines.

Actually the interface does not really simulate a wind tunnel. It just enables the user to specify selected (fixed) val-

ues for the stream conditions instead of letting them automatically being calculated. Typical free-stream conditions to be specified are the velocity V_∞, the density ρ_∞, the temperature T_∞, and the specific heat ratio γ_∞. Due to real gas effects this might be not sufficient to model the real wind tunnel conditions exactly. For the actual comparisons the numerical conditions were adjusted to reproduce the real density and temperature, and approximately also the specific heat ratio and the cold wall heat flux, resulting in following values [5]:

Table 1. Free-stream conditions used in the SCARAB wind-tunnel mode for comparison with wind tunnel measurements.

Velocity V_∞ [m/s]	3606
Density ρ_∞ [kg/m^3]	$6.7 \cdot 10^{-4}$
Temperature T_∞ [K]	730
Specific heat ratio γ_∞	1.4

Fig. 6 shows the temperature history in CFRP for 20 internal layers (layer thickness: 1 mm), computed with the SCARAB wind tunnel mode. Fig. 7 shows the temperatures computed by Kuch with his 1D method [2], and the temperatures measured in the wind tunnel probe at the surface and at 5 and 15 mm distance to the surface.

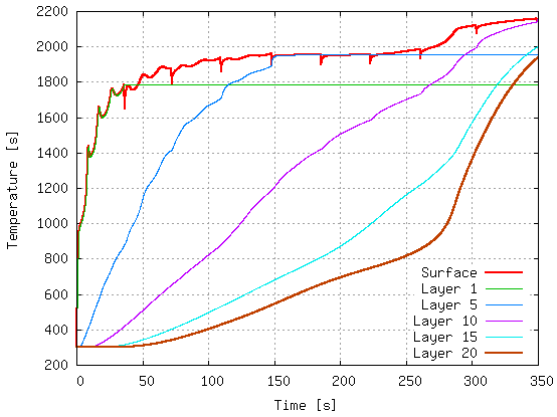

Figure 6. Computed temperatures in different layers in CFRP (total: 20 layers).

As expected the temperatures computed with the different codes are very similar, with the SCARAB values being slightly lower. The surface temperature rises very fast in the beginning, then levelling off when the radiation equilibrium is reached. The computed and measured curves corresponding to 15 mm below the surface show qualitatively similar behaviour. A characteristic feature showing up in both curves is the bend at about 250 seconds. The corresponding curves for 5 mm below the surface are quite different especially in the beginning, where the computed temperature increases very quickly, while the measured value shows only a slow increase. Nevertheless, after about 180 seconds the computed ablation is 5 mm. At the same time the measured curve ends due to the failure of the thermocouple.

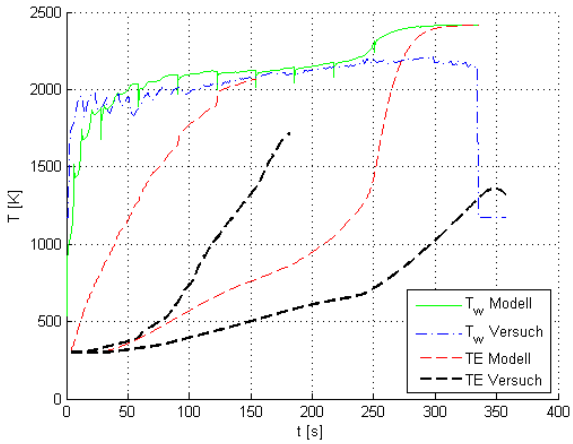

Figure 7. Measured temperatures in the wind tunnel tests compared to the 1D ablation model calculations of Kuch [2]. The curves labelled "Modell" are the temperatures computed in the surface layer (Tw, green) and for layer 5 (TE, left, red) and 15 (TE, right, red). The curves labelled "Versuch" are measured values at the surface (Tw, blue) and with the thermocouples at 5 mm (TE, left, black) and at 15 mm below the surface (TE, right, black).

Fig. 8 shows the computed mass loss of epoxy (by pyrolysis) and char (by oxidation and recession). It shows that the bend found in Fig. 7 corresponds to a complete demise of the epoxy. Comparing the char mass with the experiment (15 g at 180 s, 13.3 g at 255 s, 8.6 g at 335 s [4]) the agreement is very good for the first two values, but only fair for the last.

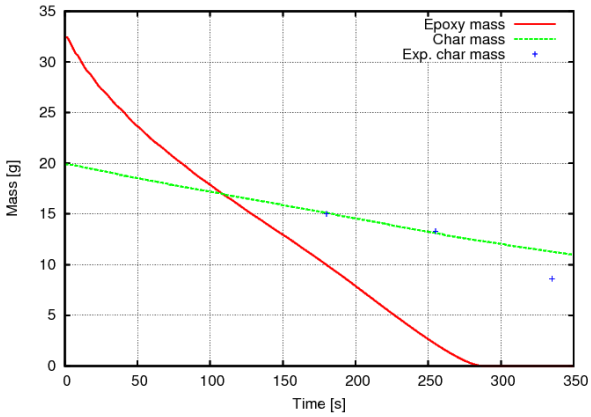

Figure 8. Computed mass of epoxy and char in CFRP with 20 internal layers

3.2. ROSAT Re-entry

ROSAT was a german X-ray satellite, launched in 1990. It was operational until 1999, then it continuously de-

cayed from its initial orbital altitude of 580 km and finally impacted on ground in 2011. In 2001 HTG performed a first SCARAB analysis of an uncontrolled ROSAT re-entry [6]. The analysis was repeated with an updated model of ROSAT in 2003 [7]. Both studies were performed well ahead of the expected re-entry date some ten years later. With the re-entry date approaching another analysis was performed in 2011, just a few months before the actual re-entry date [8]. During this analysis, besides using the most recent SCARAB version and an updated geometric model, the modelling of CFRP was updated as described in the present paper.

In the following the SCARAB simulations of 2001-2011 are compared. Tab. 2 summarizes the detail of modelling for the different cases.

Table 2. Number of modelling parts used in the different simulations.

Year	Parts	Vol.panels	Surf.panels	Grid points
2001	272	50629	123116	61824
2003	688	72424	185808	93822
2011	726	72016	201500	102124

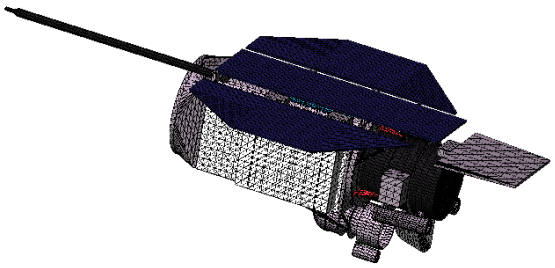

Figure 9. Geometry of ROSAT for the 2011 simulation.

Fig. 10 shows the computed initial flight altitude as function of time for the four simulations carried out in 2001, 2003, and 2011 (without+with ablation). Starting with the same initial state vector, differences in the geometric modelling and minor differences in the modelling of the environment are causing the trajectories to deviate with time. The curves end at first fragmentation, i.e. when something breaks off.

Fig. 11 shows the maximum (stagnation point) heat flux for the main fragment. The main fragment is defined as the heaviest fragment being generated during all fragmentations. Due to the different times of entry into the deep atmosphere (cf. Fig. 10) the peak heating is reached at different times as well. According to expectation, the peak heat flux decreases with increasing entry duration (flatter flight path angle). An exception is the simulation with the new ablation model. Here the peak heat flux is lower than expected according to this rule. The main reason for this is the blowing factor (cf. Eq. 9). In the actual case it reduces the effective heat flux by approximately 25%.

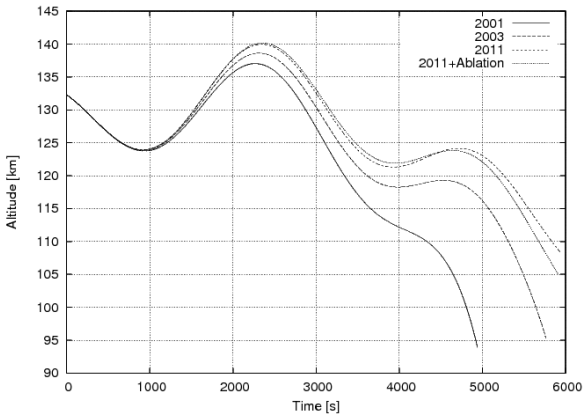

Figure 10. Flight altitude up to first fragmentation. The first fragmention occurs in the order '2001', '2003', '2011+Ablation', '2011'. The 2011 simulations cross at 4500 seconds.

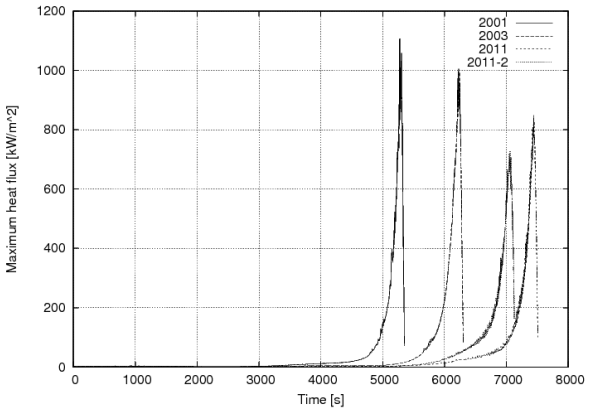

Figure 11. Maximum heat flux to the main fragment. The maximum values are reached in the order '2001', '2003', '2011-2' (with ablation), '2011' (without ablation).

Tab. 3 summarizes in short the calculated ground risk for the different simulations. In all cases the main fragment reaching ground has a mass of 50% or more of the initial mass. This is mainly due to the highly heat-resistant Zerodur glass components of the X-ray mirrors. A comparison between the early simulations (2001+2003) and the later simulations (2011) shows a reduced ground risk for the latter, which is due to a reduced number of surviving fragments. The introduction of the new ablation model decreases the ground risk further, at the cost of a larger main fragment. The geometries of the surviving main fragments for the 2003 and 2011 simulations are shown in Figs. 12-14 (not to scale). Tab. 4 compares the along-track dispersion of the surviving fragments for the three simulations in 2003 and 2011. The footprint is reduced in the 2011 simulation without ablation, and even further in the simulation with ablation. Also compared in this table are the ground track lengths without the front boom (cf. Fig. 9). The front boom is the first fragment

which survives the re-entry. Its break-off altitude is also shown in Tab. 4. Since it is quite high and the boom is quite light, it increases the total ground track length considerably. It is interesting to note that in the case with ablation the total ground track length of the fragments is shorter than for the case without ablation (due to the late break-off of the boom), but it is longer without the boom.

Table 3. Ground risk

Simulation	Initial mass [kg]	Main fragment mass [kg]	Casualty area [m^2]
2001	2410	1267	31.8
2003	2430	1334	31.4
2011	2374	1234	22.9
2011-2	2401	1564	19.7

Table 4. Fragment ground track length

Simulation	Ground track [km]	Ground track w/o boom [km]	Boom sep. altitude [km]
2003	1625	690	91.3
2011	1347	369.5	89.0
2011-2	775.8	529.4	78.7

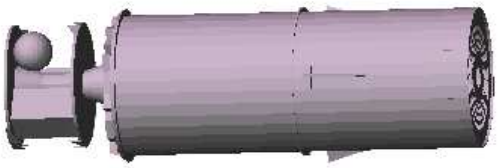

Figure 12. Main fragment geometry: Simulation 2003.

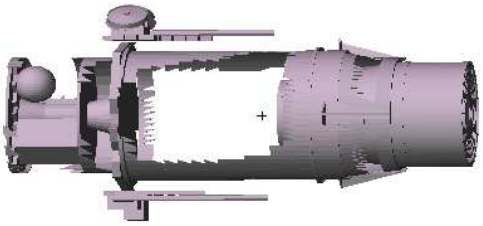

Figure 13. Main fragment geometry: Simulation 2011 (no ablation).

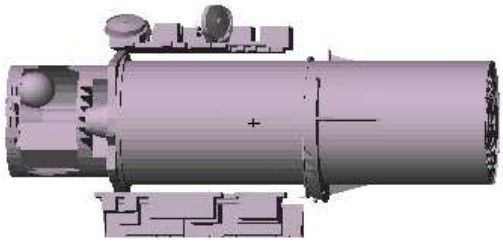

Figure 14. Main fragment geometry: Simulation 2011-2 (with ablation).

4. CONCLUSIONS

To enhance the accuracy of the survivability prediction of the SCARAB software a much more detailed model than before of CFRP, which is a prominent material constituent of many spacecraft, was developed, implemented and tested. Comparison with wind tunnel tests showed good qualitative agreement for temperature and mass loss, but amendable quantitative agreement. Application to the simulation of the ROSAT re-entry showed in general a reduction of the ground risk.

5. ACKNOWLEDGEMENT

The work presented in this paper was largely supported by the German Aerospace Center with contract no. 50 RM 1008.

REFERENCES

1. Lips, T., Fritsche, B., Koppenwallner, G., Klinkrad, H. & Toussaint, M. (2007). Re-entry Risk Assessment for Launchers – Development of the new SCARAB 3.1L. Second IAASS Conference, Chicago.
2. Kuch M. (2011). Entwicklung eines Modells für die ablative Zerstörung von Kohlefaser-Epoxy Komposites beim Wiedereintritt. Master thesis, TU Braunschweig.
3. Potts, R.L. (1995). Application of Integral Methods to Ablation Charring Erosion, A Review. *Journal of Spacecraft and Rockets*, Vol. 32, No. 2, pp. 200–209.
4. Gülhan A., Esser B. & Koch U. (2001). Untersuchungen in der L2K-Anlage zum Wiedereintrittsverhalten von Materialien des ROSAT-Satelliten. DLR IB-39113-2001C17.
5. Lips, T. & Koppenwallner, G. (2008). Re-entry Wind Tunnel Tests and ORSAT/SCARAB Comparisons. Final report, Contract no. 50 JR 0684, HTG report 08-01.
6. Lips, T. & Koppenwallner, G. (2002). Analysen für die Überlebenswahrscheinlichkeit des gesamten Satelliten ROSAT beim Wiedereintritt in die Erdatmosphäre. HTG report 02-01.
7. Lips, T. (2003). ROSAT Re-entry Analysis I, HTG-TN-03-10.
8. Fritsche, B. (2012). ROSAT Wiedereintrittsrechnungen mit SCARAB in Verbindung mit Zusatzentwicklungen zur Verbesserung der Vorhersagegenauigkeit. Final report, Contract no. 50 RM 1008, HTG-TR-12-03.